CrossMark

Downloaded from https://www.cambridge.org/core. TU Berlin Universitaetsbibliothek, on 06 Apr 2020 at 10:05:56, subject to the Cambridge Core terms of use, available at https://www.cambridge.org/core/terms. https://doi.org/10.1557/jmr.2017.144

ARTICLE

Physical properties and lattice dynamics of bixbyite-type V_2O_3

Dominik A. Weber[a)]
Institut für Chemie, Tecnische Universität Berlin, 10623 Berlin, Germany; and Physikalisch-Chemisches Institut, Justus-Liebig-Universität Gießen, 35392 Gießen, Germany

Christian Schwickert
Institut für Anorganische und Analytische Chemie, Universität Münster, 84149 Münster, Germany

Anatoliy Senyshyn
Heinz Maier-Leibnitz Zentrum, Technische Universität München, 85748 Garching, Germany

Martin Lerch
Institut für Chemie, Tecnische Universität Berlin, 10623 Berlin, Germany

Rainer Pöttgen
Institut für Anorganische und Analytische Chemie, Universität Münster, 84149 Münster, Germany

(Received 8 December 2016; accepted 30 March 2017)

Some time ago, we reported the synthesis of bixbyite-type V_2O_3, a new metastable polymorph of vanadium sesquioxide. Since, a number of investigations followed, dealing with different aspects like electronic and magnetic properties of the material, the deviation from ideal stoichiometry or the preparation of nanocrystals as oxygen storage material. However, most of the physical properties were only evaluated on a theoretical basis. Here, we report the lattice dynamics and physical properties of bixbyite-type V_2O_3 bulk material, which we acquired from physical property measurements and neutron diffraction experiments over a wide temperature range. Besides attributing different possible orientations of the magnetic moments for V1 and V2 to the identified antiferromagnetic (AFM) ground state with a Néel temperature of 38.1(5) K, we use a first order Grüneisen approximation to determine lattice-dependent parameters for the relatively stiff cubic lattice, and, amongst others identify the Debye temperature to be as low as 350 ± 65 K.

I. INTRODUCTION

Because of their structural diversity, abundant physical and chemical properties, and numerous potential applications, vanadium-based materials hold an exceptional position amongst transition metal-based compounds. Besides their use in electronic and optical devices,[1] chemical sensors,[2] as catalysts,[3,4] and as cathode materials for high energy density lithium ion batteries,[5–7] even binary vanadium oxides, due to their unique behavior, have been subject to various investigations. In particular, a large number of experimental and theoretical studies have already been conducted on the thermodynamically stable vanadium sesquioxide, as it presents a model system for a Mott–Hubbard transition.[8–10] At low temperatures, this polymorph of V_2O_3 is an antiferromagnetic (AFM) insulator, crystallizing in a monoclinic structure (M1). At around 170 K it transforms into a paramagnetic conductor, undergoing a structural phase transition to the well-known rhombohedral corundum-type structure with a notably large *c*/*a* ratio of 2.823.[9–14]

Regarding the inimitable characteristics of thermodynamically stable V_2O_3, the investigation of the physical properties of additional polymorphs of V_2O_3 is of fundamental interest. A few years ago, we synthesized a new metastable polymorph of vanadium sesquioxide that crystallizes in the bixbyite-type structure (space group $Ia\bar{3}$).[15] This polymorph of V_2O_3 has since been the subject of numerous investigations, including the synthesis of particles with urchin-like morphology by thermal decomposition of vanadyl ethylene glycolate[16] or of phase pure nanocrystals by a colloidal route.[17] Interestingly, these nanocrystals were only recently shown to reversibly incorporate up to two additional oxygen atoms per unit cell onto vacant anion sites in the crystal structure,[18] fitting well with the predictions on intrinsic defects that we studied on density-functional theory (DFT) level.[19] These vacant sites are located at the 16*c* Wyckoff position in the bixbyite structure, which can be treated as an anion-deficient 2 × 2 × 2 supercell of the fluorite structure with a quarter of the anions removed (Fig. 1). While the cations are distributed over two symmetry-inequivalent positions, 8*b* and 24*d*, respectively, the anions populate the 48*e* positions, giving a total of 80 atoms per unit cell ($Z = 16$).

Shortly after our first contribution on the new polymorph of V_2O_3, we theoretically studied the structural,

Contributing Editor: Michael E. McHenry
[a)]Address all correspondence to this author.
e-mail: dominik.weber@phys.chemie.uni-giessen.de
DOI: 10.1557/jmr.2017.144

 © Materials Research Society 2017

Downloaded from https://www.cambridge.org/core. TU Berlin Universitaetsbibliothek, on 06 Apr 2020 at 10:05:56, subject to the Cambridge Core terms of use, available at https://www.cambridge.org/core/terms. https://doi.org/10.1557/jmr.2017.144

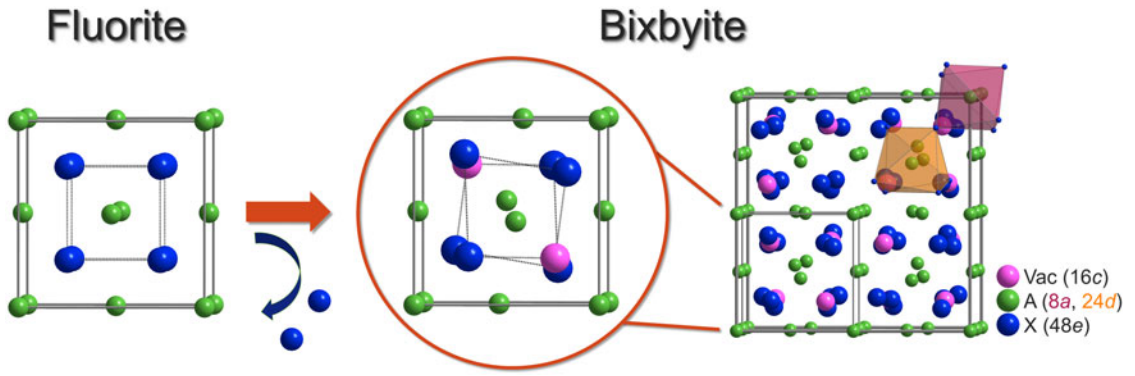

FIG. 1. Structural relationship between fluorite *fcc* and bixbyite *bcc* structure. Besides 16 ordered anion vacancies (16*c* position, pink), the bixbyite structure comprises two symmetry-inequivalent cation positions (8*a*, red and 24*d*, orange, respectively) as well as 48 equivalent anion positions (48*e*, blue). For V_2O_3 in this structure type, reversible incorporation of up to two additional oxygen atoms per unit cell is possible, utilizing the 16*c* position.

thermodynamic, and electronic properties of the new phase amongst other possible polymorphs and found strong indications for the formation of a band gap in an AFM ground state.[20]

Up to that point, we were not able to isolate the phase-pure material and physical property measurements were therefore carried out on samples that contained at least 18 wt% of the corundum-type polymorph as a side phase. Hence, we were not able to ascribe the observed phenomena for these samples solely to the bixbyite-type phase. Here, we present results of in-depth studies of the physical properties of phase-pure bixbyite-type V_2O_3 bulk material, which we recently were able to synthesize,[21] and link them to results from temperature-dependent neutron and X-ray diffraction. For the first time, we determine the lattice dynamics of bixbyite-type V_2O_3, and confirm the AFM order of the material predicted by quantum-chemical calculations.

II. EXPERIMENTAL SECTION

A. Sample preparation

All reactions were carried out in a conventional tube furnace equipped with a corundum tube with an inner diameter of 50 mm. The reaction gas was led directly onto the sample by a second corundum tube with an inner diameter of 5 mm. The flow rate of the reaction gas [40 vol% H_2 in Ar (both Air Liquide, Dusseldorf, Germany), gas stream piped through a water-filled washing flask] was regulated with a parallel arrangement of two digital volumetric mass flow controllers (Brooks Instrument LLC, Hatfield, Pennsylvania) and set to 10 L/h. For each batch, 500 mg of $V_2F_6{\cdot}4H_2O$ or $V_2F_6{\cdot}6H_2O$ (synthesized from vanadium powder and aqueous H_2SiF_6[22]) were placed in a small alumina boat inside the tube and heated under flowing reaction gas for 2 h at 753 K, applying a heating ramp of 300 K/h. After the dwell was complete, the furnace was swung open to allow for fast heat dissipation. Simultaneously, the atmosphere was changed to 10 L/h of dry argon (5.0, Air Liquide). After cooling, the grayish-black product was obtained without further treatment.

B. Basic characterization

The obtained products were characterized by X-ray powder diffraction (PANalytical X'Pert PRO MPD with Cu K_α radiation, PIXcel detector, PANalytical B.V., Almelo, The Netherlands) at ambient temperature. Structural refinements were performed in the same manner as described in the neutron diffraction section. Quantitative analysis of the oxygen content was performed by the well-established hot gas extraction method (LECO TC300/EF300, LECO Corp., St. Joseph, Michigan), using zirconia and corundum-type V_2O_3 as standards. The experimental error for this method amounts to ≈2% of the presented values (i.e., $V_2O_{3\pm0.06}$).

C. Physical property measurements

Magnetic measurements were performed in the temperature range of 2.5–305 K, using a Quantum Design Physical-Property-Measurement-System (Quantum Design, San Diego, California) with magnetic flux densities of up to 80 kOe. All measurements were carried out using the VSM option by packing the powdered sample (15.642 mg) in a polypropylene capsule and attaching it to a brass sample holder. A heat capacity measurement was performed in the temperature range of 2.1–305 K, using the same Quantum Design Physical-Property-Measurement System. For the measurement, a compact sample was prepared and embedded into Apiezon N grease (Apiezon Products, M&I Materials Ltd., Manchester, United Kingdom) to ensure thermal coupling with the sample holder platform.

D. Neutron diffraction

Elastic coherent neutron scattering experiments were performed at the Heinz Maier-Leibnitz Zentrum

Downloaded from https://www.cambridge.org/core. TU Berlin Universitaetsbibliothek, on 06 Apr 2020 at 10:05:56, subject to the Cambridge Core terms of use, available at https://www.cambridge.org/core/terms. https://doi.org/10.1557/jmr.2017.144

(Garching near Munich, Germany) on the high-resolution diffractometer SPODI.[23] Monochromatic neutrons (λ = 1.5482 Å) were obtained at a 155° take-off angle, using the 551 reflection of a vertically-focused composite Ge monochromator. A vertical position-sensitive multidetector (300 mm effective height) consisting of 80 ^{3}He tubes and covering an angular range of 160 deg. 2θ was used for the data collection. Measurements were performed in Debye–Scherrer geometry. The powder sample (approximately 1 cm^3 in volume) was filled into a thin-walled (0.15 mm) vanadium can of 10 mm in diameter, which was then mounted in the top-loading closed-cycle refrigerator. Helium 4.6 was used as a heat transmitter. The temperature was measured instantaneously, using two thin film resistance cryogenic temperature sensors (Cernox™, Lake Shore Cyrotronics Inc., Westerville, OH) and controlled by a temperature controller from LakeShore Cyrotronics Inc. Two-dimensional powder diffraction datasets were collected at fixed temperatures in the range of 4–320 K. Depending on the temperature, different exposure times were applied, *i.e.*, to reveal the weak effect of magnetism in V_2O_3, the data at 4 K were collected for 21 h, whilst shorter data collection times were applied at 60 K (10 h) and 300 K (5 h). Additionally, a number of diffraction patterns with short exposure times (30 min) was collected at fixed temperatures in the temperature range 4, 10, 20, 30, … 320 K. The collected 2D diffraction patterns were then corrected for geometrical aberrations and curvature of the Debye–Scherrer rings.[24]

Rietveld refinements were carried out using the software package FullProf Suite.[25,26] The peak profile shape was modeled by a pseudo-Voigt function. The background of the diffraction pattern was fitted using a linear interpolation between selected data points in nonoverlapping regions. To deduce the evolution of the lattice parameters, the Rietveld method was applied for the analysis of the neutron data with no vanadium contribution, taking into account the anomalously low coherent neutron scattering length of the ^{51}V isotope, which dominates in natural vanadium (99.75 %). For the coherent nuclear part of the scattering process, this low scattering length causes "blindness" of neutrons against vanadium. The magnetic form factor, on the other hand, depends on the magnetization distribution of the atoms, and therefore the detection of magnetic moments on natural vanadium atoms using nonpolarized neutron diffraction, is possible. The scale factor, the lattice parameter, the fractional coordinates of the atomic sites, and their isotropic displacement parameters, the zero angular shift, the profile shape parameters and the half width (Caglioti) parameters were varied during the fitting. Selected exemplary results for the data acquired at T = 4 K are presented in Table I together with the data from X-ray diffraction at room temperature.

TABLE I. Experimental structural parameters of bixbyite-type V_2O_3 (obtained from neutron diffraction data at T = 4 K and X-ray diffraction data at T = 298 K). The space group is $Ia\bar{3}$ (No. 206). The structural data were modeled for the V1, V2, and O1 ions occupying the Wyckoff positions 8*a* [0, 0, 0], 24*d* [*x*, 0, 1/4] and 48*e* [*x*, *y*, *z*]. Numbers in parentheses give estimated standard deviations in the last significant digit.

Neutron diffraction @ 4 K	a = 9.3824(2) Å, V = 825.93(3) Å^3			
Atom site	*x/a*	*y/b*	*z/c*	B_{iso}, Å^2
V1	0	0	0	0.6(4)
V2	0.289(2)	0	1/4	0.6(4)
O1	0.1394(1)	0.1290(2)	−0.0963(1)	0.82(2)
μ = 0.4(1) μ_B; R_p: 1.59%, R_{wp}: 2.15%, R_{exp}: 0.59%, χ^2: 13.3				

X-ray diffraction @ 298 K	a = 9.3936(2) Å, V = 828.90(3) Å^3			
Atom site	*x/a*	*y/b*	*z/c*	B_{iso}, Å^2
V1	0	0	0	0.80(5)
V2	0.28173(6)	0	1/4	0.95(4)
O1	0.1426(2)	0.1286(3)	−0.0952(4)	0.45(4)
R_p: 1.60%, R_{wp}: 2.13%, R_{exp}: 1.91%, χ^2: 1.24				

III. RESULTS AND DISCUSSION

A. Syntheses and crystal chemistry

Phase-pure bixbyite-type vanadium sesquioxide was successfully obtained as described in the experimental section. Quantitative oxygen analysis of the here-presented samples resulted in 31.8 wt% oxygen, leading to a composition of $V_2O_{2.98}$. This result is in fair agreement with the ideal bixbyite stoichiometry. The grayish-black product was structurally characterized using X-ray powder diffraction. The results of the Rietveld refinement are given in Fig. 2 and Table II.

The lattice parameter of a = 939.64(2) pm shows no significant deviation (≈0.02%) from the one we reported in our first contribution [939.47(2) pm].[15] Furthermore, the determined atomic parameters are in good agreement with the formerly reported ones.

B. Magnetic properties

The temperature dependent inverse susceptibility [$\chi^{-1}(T)$ data] of V_2O_3, measured with magnetic flux densities of 1 and 10 kOe (almost identical temperature dependence) is depicted in Fig. 3(a). The inset of Fig. 3(a) shows the low temperature regime of a temperature dependent susceptibility measurement in *zero-field-cooled* (ZFC)/*field-cooled* (FC) mode acquired with a low magnetic flux density of 100 Oe.

A least-squares fit of the inverse magnetic susceptibility data of the 10 kOe measurement in the temperature range of 100–300 K with a modified Curie–Weiss law

Downloaded from https://www.cambridge.org/core. TU Berlin Universitaetsbibliothek, on 06 Apr 2020 at 10:05:56, subject to the Cambridge Core terms of use, available at https://www.cambridge.org/core/terms. https://doi.org/10.1557/jmr.2017.144

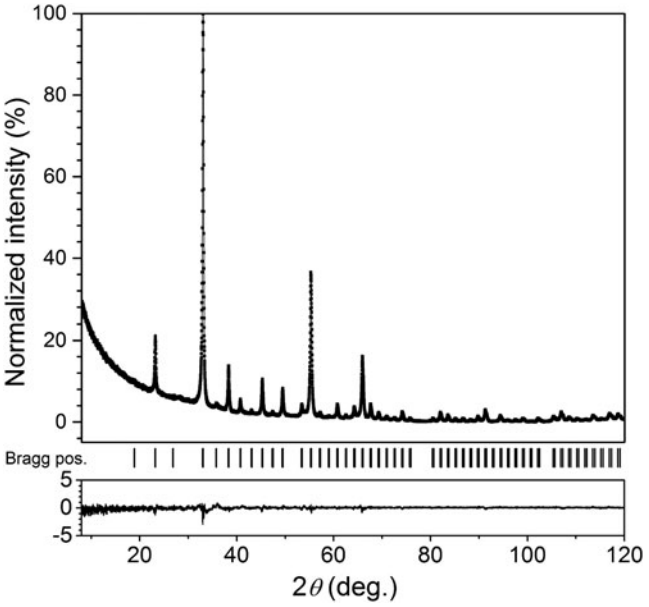

FIG. 2. X-ray powder diffraction diagram of phase-pure bixbyite-type V_2O_3 at room temperature with graphical results of the Rietveld refinement.

TABLE II. Numerical results of the Rietveld refinement against X-ray diffraction data at room temperature.

Composition	V_2O_3
Structure type	Bixbyite
Space group	$Ia\bar{3}$
Lattice parameter	a = 939.64(2) pm
Formula units	16
Unit cell volume (normalized to one formula unit)	51.81 × 10^6 pm^3
Calculated density	4.80 g/cm^3
Diffractometer	PANalytical X'Pert PRO MPD
Wavelength	Cu K_α [λ_1 = 154.056 pm; λ_2 = 154.539 pm; $I(\lambda_2/\lambda_1 = 0.5)$]
Profile points	8839
2θ range	5–120°
R_{Bragg}	0.021
R_{wp}	0.021
R_{exp}	0.019
S (Goodness of fit)	1.11

$$\chi^{-1} = \chi_0{}^{-1} + \frac{T - \theta}{C}$$

yielded an experimental magnetic moment of μ_{exp} = 1.72(1) μ_B/vanadium-atom, a Weiss constant of $\theta_P = -71.4(5)$ K and a temperature independent contribution $\chi_0 = 6.49(1) \times 10^{-4}$ emu/mol, where χ_0 takes into account Van-Vleck and core corrections, as well as paramagnetic contributions of conduction band electrons. The experimental magnetic moment corresponds to the value for a free V^{4+} ion (1.73 μ_B), assuming a spin-only high-spin state rather than a V^{3+} state. The Weiss

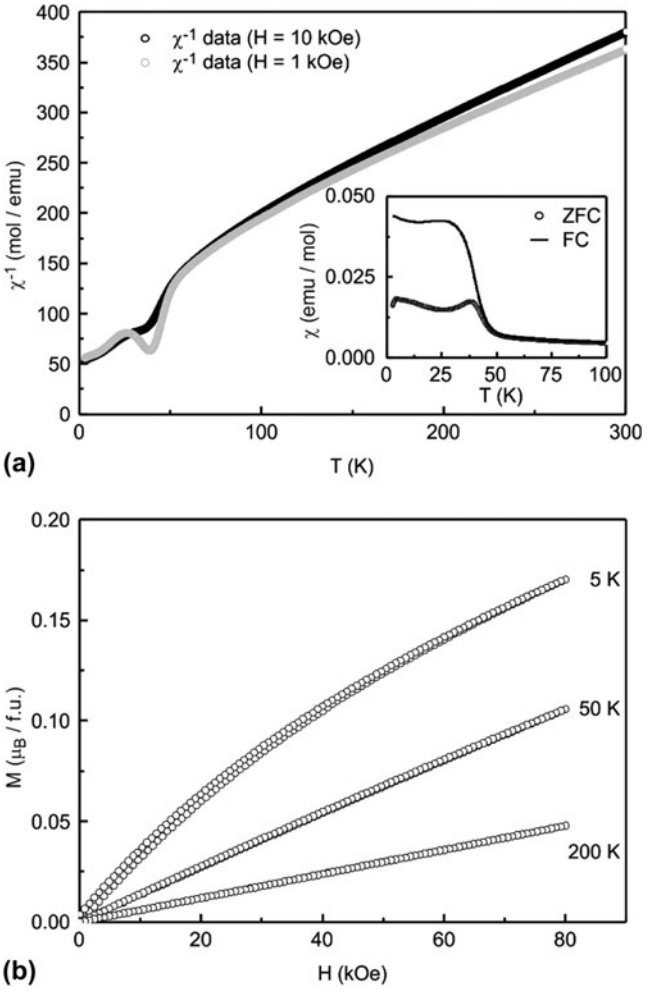

FIG. 3. (a) Temperature dependent inverse magnetic susceptibilities of cubic V_2O_3 measured at magnetic flux densities of 1 and 10 kOe. The inset depicts the low temperature regime of a temperature dependent magnetic susceptibility measurement of the V_2O_3 sample in ZFC/FC mode with a magnetic flux density of 100 Oe. (b) Magnetization isotherms of cubic V_2O_3 measured at 5, 50 and 200 K with magnetic flux densities up to 80 kOe.

constant is indicative of dominating AFM interactions in the paramagnetic domain. As will be discussed later, this behavior can be explained by frustration of the magnetic moments, leading to short-range order.

The Néel temperature T_N = 38.1(5) K was determined from the ZFC/FC measurement. As expected for paramagnetic materials, the magnetization isotherms [Fig. 3(b)] above the observed ordering temperature show a linear increase with the applied field. The 5 K isotherm exhibits no tendency of saturation, while showing a small hysteresis. From the course of the FC measurement along with the minute hysteresis of the 5 K magnetization isotherm [Fig. 3(b)], a canted, weakly ferromagnetic ground state has to be assumed.

The temperature dependence of the specific heat of the V_2O_3 sample is presented in Fig. 4. We observe no anomaly in the temperature window, where magnetic

Downloaded from https://www.cambridge.org/core. TU Berlin Universitaetsbibliothek, on 06 Apr 2020 at 10:05:56, subject to the Cambridge Core terms of use, available at https://www.cambridge.org/core/terms. https://doi.org/10.1557/jmr.2017.144

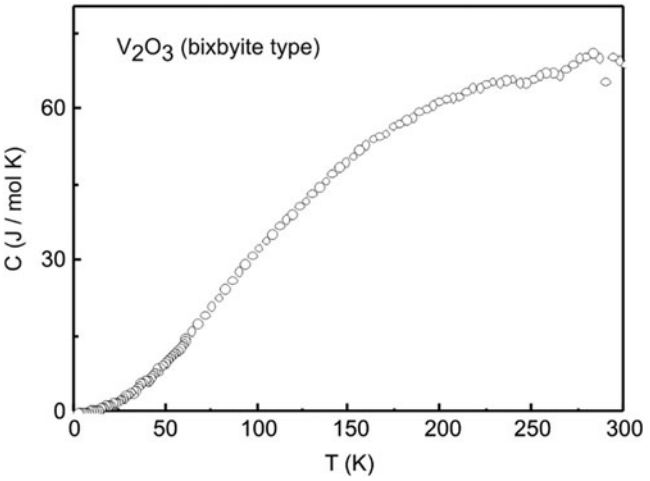

FIG. 4. Temperature dependence of the specific heat of cubic V_2O_3 measured in zero magnetic field.

ordering is evident in the susceptibility data. In view of the small value of the ordered moment, this is not surprising (see also the neutron diffraction data below). Thus, we only find a small value for the entropy change that is associated with the magnetic ordering process. This behavior is similar to that observed for Sr_2IrO_4.[27] Another important point concerns small degrees of vacancies or inhomogeneities within the oxygen substructure, which can also hamper long-range ordering due to both randomness and frustration of magnetic moments.

C. Neutron diffraction studies

The analysis of the neutron powder diffraction data at different temperatures revealed only reflections that are characteristic for a body centered cubic lattice (weak traces of aluminum from the walls of the closed-cycle refrigerator were present in the diffraction patterns at all temperatures), indicating the isostructurality of V_2O_3 within the whole studied temperature range. Due to the low coherent scattering length of vanadium in the natural isotope blend, its localization in the lattice on the basis of neutron data is quite challenging. An attempt to include vanadium into the refinement of the neutron powder diffraction data at room temperature resulted in a reduction of the *R* factors by approximately 0.1–0.2%. The accuracy of the vanadium localization from neutron and X-ray diffraction data can be illustrated by the *x/a* fractional coordinate for the V2 atom: the neutron diffraction experiment revealed $x/a = 0.289(2)$, whereas X-ray powder diffraction enabled a determination of the V2 position at $x/a = 0.28173(6)$ (see Table I), which demonstrates an about two orders of magnitude better resolution for the latter.

The temperature dependent evolution of the lattice parameter of cubic V_2O_3 was determined by Rietveld analysis of the "short" neutron powder diffraction data sets collected in the temperature range between 4 and 320 K. The resulting thermal dependence of the lattice parameter was obtained by combining the obtained results with high-temperature lattice parameters, we obtained earlier.[15] The results are shown in Fig. 5. Both, low- and high-temperature data sets were found to be in good agreement, thus indicating that the structure of cubic V_2O_3 is quite stiff to temperature changes, i.e., heating from 4 to 850 K resulted in a minor increase of the lattice parameter by approximately 0.04 Å (≈0.4%).

The first order Grüneisen approximation was applied to interpret the obtained temperature dependence of the structure of cubic V_2O_3. It can be described as

$$V(T) = V_0 + \frac{\gamma}{K_T} U(T) \quad , \tag{1}$$

where V_0 denotes the hypothetical cell volume at zero temperature, γ is the Grüneisen constant, K is the bulk modulus, and U is the internal energy of the system. Both, the Grüneisen constant and the bulk modulus are supposed to be temperature-independent and the Debye approximation for the internal energy U in Eq. (1) has the form

$$U(T) = U_D(T) = \left[9Nk_BT\left(\frac{T}{\theta_D}\right)^3 \int_0^{\theta_D/T} \frac{x^3}{e^x - 1} dx \right] \quad , \tag{2}$$

with the characteristic temperature θ_D (Debye temperature), the number of atoms in the unit cell N and the Boltzmann constant k_B, providing a reasonable description for the cell volume, similar to the procedure applied to data on FeSi.[28]

Least-squares nonlinear fitting of the experimental data according to Eqs. (1) and (2) resulted in an adequate description of the lattice parameter of cubic V_2O_3 by the first order Grüneisen approximation with $V_0 = 825.8 \pm 0.1$ Å^3, $\gamma/K = 4.4 \pm 0.1 \times 10^{-12}$ Pa^{-1} and $\theta_D = 350 \pm 65$ K (see Fig. 5). The cubic modification of V_2O_3 is characterized by a relatively low Debye temperature; for the rhombohedral corundum-type modification of V_2O_3, a Debye temperature ranging from 575 to 643 K has been reported.[29] On the other hand, the compound shows a weak thermal expansion: The thermal expansion coefficient calculated as $a_l(T) = \frac{\partial \ln l(T)}{\partial T} = \frac{1}{3}\frac{\partial \ln V(T)}{\partial T}$ yielded $a_l \sim 5.8$ K^{-1} at the proximity of the phase transition to the corundum-type phase at approximately 823 K.[15]

Besides the weak anharmonicity effects, cubic V_2O_3 is known to order magnetically.[15] A previously performed evaluation of the lattice dimensions versus temperature revealed no sufficient magnetoelastic couplings to the lattice in V_2O_3. Additionally, the inspection of the "short" neutron powder diffraction data sets provided no

Downloaded from https://www.cambridge.org/core. TU Berlin Universitaetsbibliothek, on 06 Apr 2020 at 10:05:56, subject to the Cambridge Core terms of use, available at https://www.cambridge.org/core/terms. https://doi.org/10.1557/jmr.2017.144

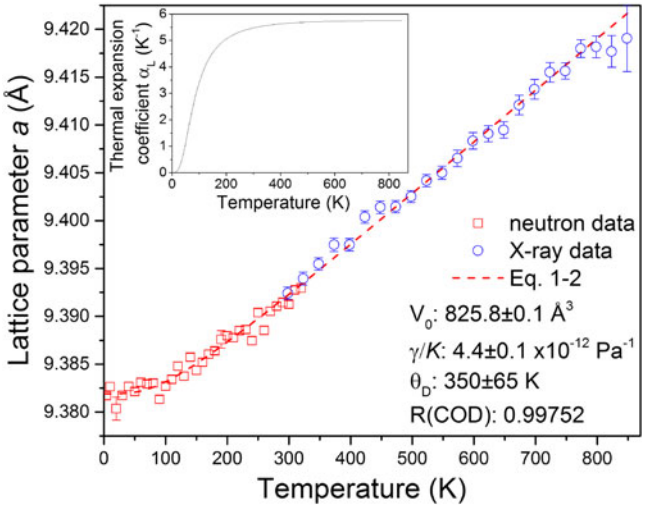

FIG. 5. Temperature evolution of the lattice parameter in cubic V_2O_3; neutron data are shown in red, X-ray data[15] in blue color. The scattered lines correspond to the results of data fitting by Eqs. (1) and (2); the calculated thermal expansion coefficient is shown in the inset.

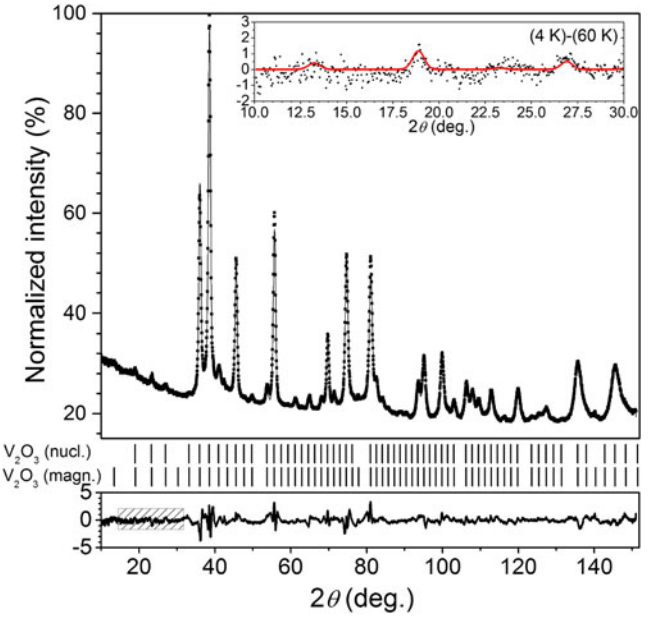

FIG. 6. Graphical results of the Rietveld refinement against neutron powder diffraction data of bixbyite-type V_2O_3 at 4 K; calculated positions of Bragg reflections for the nuclear and the magnetic contribution are shown by the top and bottom row of vertical tick marks. The inset illustrates the low temperature section of the normalized differential diffraction patterns collected at 4 and 60 K. The red line corresponds to the model for the magnetic contribution.

visible indication for a long range magnetic order below T_C. Only a detailed evaluation of the "long" diffraction data sets collected at 4 and 60 K yielded weak additional neutron intensities on top of the nuclear reflections at low angles (see Fig. 6), which can be an evidence for long range magnetic ordering, with a magnetic lattice that has identical metrics as the nuclear one (propagation vector $\mathbf{k} = [0, 0, 0]$).

Bixbyite-type V_2O_3 comprises two crystallographically inequivalent vanadium positions. An analysis of the magnetic representations was performed by the Bertaut method[30] implemented in the BasIreps software,[31] revealing 8 irreducible representations that form a little group $\mathbf{G_k}$ (coinciding with the $Ia\bar{3}$ symmetry and leaving the propagation vector $\mathbf{k}$ invariant). Due to the weak thermal expansion and the weak magnitude of the observed magnetic effects, the evaluation of the magnetic structures was performed on the differential diffraction pattern in the 2θ angular range of 10–35°. Magnetic structure models based on 1D irreducible representations were constructed in different configurations, but their refinement did not yield an adequate description of the magnetic intensities. 3D irreducible representations, on the other hand, apply fewer constraints to the orientation and magnitude of the magnetic moments in bixbyite-type V_2O_3. However, no consistent conclusion about the magnetic structure can be made from the least-squares minimization due to convergence and correlation issues, which can be related to the restrictions applied to the highly symmetric lattice regarding determination of the magnetic moment orientations from powder diffraction data.[32]

To describe the obtained residual intensities, the iterative approach (assuming a 2D collinear AFM structure for V_2O_3) has been applied. The magnetic moments for the V^{3+} sites were aligned in 2 states: either alongside or opposite to the c axis. With 16 formula units in bixbyite-type V_2O_3, the number of possible configurations is limited to 2.[16] An assumption about the AFM ground state at 4 K (supported by the magnetization measurements) further reduces the number of configurations to 12,870. Each configuration with a predefined orientation of the magnetic moments was evaluated by Rietveld refinement, where the amplitude of the magnetic moments was constrained to be the same for both V1 and V2, and was allowed to vary.

Due to the low magnitude of the observed effects and, correspondingly, large fit residuals, the sum of the magnetic R factor and χ^2 were used as a figure of merit (the use of R_p and R_{wp} does not change the results). Four configurations (shown in Fig. 7) possessing equal values for $R_m + \chi^2$ have been identified and their accuracy cannot further be judged on the basis of the present neutron powder diffraction data (similar models can also be drawn, assuming an FM direction opposite to the c axis; indistinguishable by powder diffraction). The magnetic moments of the V1 sites have been found to be oriented ferromagnetically along the c axis, whilst the moments of the V2 sites are located either alongside or opposite to the c axis to maintain zero net magnetization. The amplitude of the magnetic moments was refined to

Downloaded from https://www.cambridge.org/core. TU Berlin Universitaetsbibliothek, on 06 Apr 2020 at 10:05:56, subject to the Cambridge Core terms of use, available at https://www.cambridge.org/core/terms. https://doi.org/10.1557/jmr.2017.144

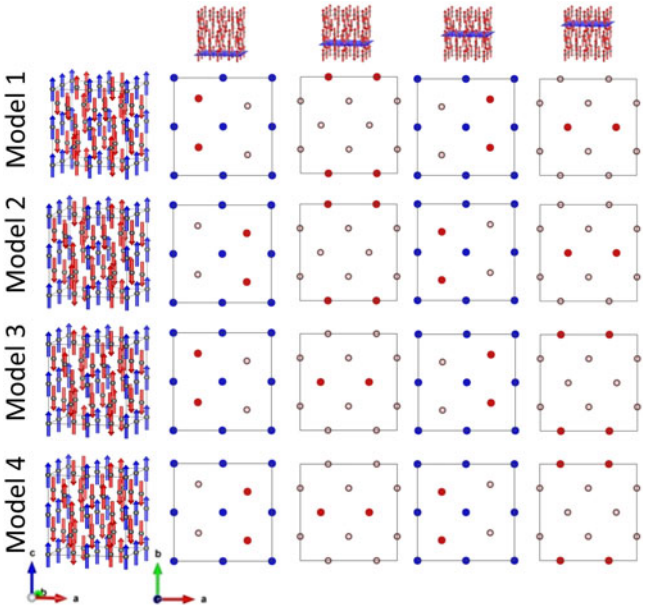

FIG. 7. Obtained variances of the collinear AFM ground state in bixbyite V_2O_3 based on Rietveld modeled data at 4 K (column 1). The magnetic moments on the V1 site are shown in blue color, magnetic moments on V2 are in red. A sketch of the magnetic moment orientation at four distinct 001 planes is shown in columns 2–5, solid points depict moment orientation along the *c* axis.

0.71(3) μ_B, using differential data and 0.4(1) μ_B, using a completed data set at 4 K. Anyways, these values are considerably lower than the expected moment for V^{3+} (approximately 2.8 μ_B[33]). We already reported some discrepancies, earlier[15] and associated them with deviations from the V^{3+} state of the vanadium ions, which we also rendered possible by theoretical calculations.[19] On the other hand, magnetic interactions may undergo a geometrical frustration in bixbyite-type V_2O_3, with the V1 and V2 ions located on the vertices of trigonal and hexagonal frameworks. One also has to mention that a constraint of the magnetic moments on V1 and V2 leads to an AFM lattice with zero net magnetization, whereas a small discrepancy in the moment amplitudes between the V1 and V2 magnetic sites (initially permitted by symmetry) may result in the appearance of a weak ferromagnetic moment. This is in excellent agreement with the absence of a lambda type anomaly in the specific heat data (Fig. 4).

IV. CONCLUSIONS

The magnetic properties of bixbyite-type V_2O_3 have been studied and revealed an experimental magnetic moment of μ_{exp} = 1.72(1) μ_B/vanadium-atom, which interestingly corresponds to a free V^{4+} ion (1.73 μ_B), rather than V^{3+}. The observed Weiss constant of $\theta_P = -71.4(5)$ K is indicative for AFM interactions in the paramagnetic domain and a canted, weakly AFM ground state seems to be present. A Néel temperature of T_N = 38.1(5) K was determined. Furthermore, only a very small value for the entropy change during magnetic ordering is present, most probably because of randomness and frustration of the magnetic moments, hampering long-range ordering in the material.

Using high-resolution neutron powder diffraction at low and intermediate temperatures, isostructurality of V_2O_3 has been confirmed in the whole temperature range from 4 to 320 K. The cubic V_2O_3 is characterized by a rather low thermal expansion in the whole range of existence (below 823 K), which can be fairly well described by a first order Grüneisen approximation. For the first time, the hypothetical zero Kelvin value for the cell volume V_0 as well as the temperature independent γ/K ratio and Debye temperature θ_D have been determined to be as large as 825.8 ± 0.1 Å^3, 4.4 ± 0.1 × 10^{-12} Pa^{-1}, and 350 ± 65 K.

Based on the iterative approach, 12,870 different AFM configurations of the V^{3+} magnetic moment arrangements adopting zero net magnetization have been evaluated using Rietveld refinements. Based on the fit residuals, four possible configurations have been chosen, where all adopt FM arrangement of the V1 magnetic moments and ferrimagnetic order of V2 (with a weak FM component opposite to that of V1). A weak ferrimagnetic component in bixbyite-type V_2O_3 can be tuned by the discrepancy of the V1 and V2 magnetic moments and the weak ferromagnetism can be attributed to the different order temperatures (and, correspondingly, saturation behavior) for the V1 and V2 magnetic ions.

Due to the weak magnitude of the ordered moments, an accurate determination of their arrangement between different vanadium sites would require neutron diffraction experiments on single crystals.

ACKNOWLEDGMENT

Financial support from the German Research Foundation (DFG) within the priority program SPP 1415 (LE 781/11-2) is gratefully acknowledged. The authors further gratefully acknowledge the financial support provided by FRM II to perform the neutron scattering measurements at the Heinz Maier-Leibnitz Zentrum (MLZ), Garching, Germany.

REFERENCES

1. J. Muster, G.J. Kini, J.G. Park, and M. Burghard: Electrical transport through individual vanadium pentoxide nanowires. *Adv. Mater.* **12**, 420 (2000).
2. P. Liu, S-H. Lee, H.M. Cheong, C.E. Tracy, J.R. Pitts, and R.D. Smith: Stable Pd/V_2O_5 optical H_2 sensor. *J. Electrochem. Soc.* **149**, H76 (2002).
3. J. Haber: Fifty years of my romance with vanadium oxide catalysts. *Catal. Today* **142**, 100 (2009).

Downloaded from https://www.cambridge.org/core. TU Berlin Universitaetsbibliothek, on 06 Apr 2020 at 10:05:56, subject to the Cambridge Core terms of use, available at https://www.cambridge.org/core/terms. https://doi.org/10.1557/jmr.2017.144

4. C. Hess: Nanostructured vanadium oxide model catalysts for selective oxidation reactions. *ChemPhysChem* **10**, 319 (2009).
5. P.P. Prosini, Y. Xia, T. Fujieda, R. Vellone, M. Shikano, and T. Sakai: Performance and capacity fade of V_2O_5–lithium polymer batteries at a moderate–low temperature. *Electrochim. Acta* **46**, 2623 (2001).
6. Y. Shi, Z.J. Zhang, D. Wexler, S. Chou, J. Gao, H.D. Abruna, H. Li, H. Liu, Y. Wu, and J. Wang: Facile synthesis of porous V_2O_3/C composites as lithium storage material with enhanced capacity and good rate capability. *J. Power Sources* **275**, 392 (2015).
7. L. Jiang, Y. Qu, Z. Ren, P. Yu, D. Zhao, W. Zhou, L. Wang, and H. Fu: *In situ* carbon-coated yolk–shell V_2O_3 microspheres for lithium-ion batteries. *ACS Appl. Mater. Interfaces* **7**, 1595 (2015).
8. N.F. Mott: *Metal-insulator Transition* (Taylor and Francis Ltd, London, 1974).
9. K. Held, G. Keller, V. Eyert, D. Vollhardt, and V.I. Anisimov: Mott–Hubbard metal-insulator transition in paramagnetic V_2O_3: An LDA + DMFT(QMC) study. *Phys. Rev. Lett.* **86**, 5345 (2001).
10. P. Hansmann, A. Toschi, G. Sangiovanni, T. Saha-Dasgupta, S. Lupi, M. Marsi, and K. Held: Mott–Hubbard transition in V_2O_3 revisited. *Phys. Status Solidi B* **250**, 1251 (2013).
11. L.W. Finger and R.M. Hazen: Crystal structure and isothermal compression of Fe_2O_3, Cr_2O_3, and V_2O_3 to 50 kbars. *J. Appl. Phys.* **51**, 5362 (1980).
12. D.B. McWhan and J.B. Remeika: Metal-insulator transition in $(V_{1-x}Cr_x)_2O_3$. *Phys. Rev. B: Condens. Matter Mater. Phys.* **2**, 3734 (1970).
13. P.D. Dernier and M. Marezio: Crystal structure of the low-temperature antiferromagnetic phase of V_2O_3. *Phys. Rev. B: Condens. Matter Mater. Phys.* **2**, 3771 (1970).
14. R.M. Moon: Antiferromagnetism in V_2O_3. *Phys. Rev. Lett.* **25**, 527 (1970).
15. D. Weber, A. Stork, S. Nakhal, C. Wessel, C. Reimann, W. Hermes, A. Müller, T. Ressler, R. Pöttgen, T. Bredow, R. Dronskowski, and M. Lerch: Bixbyite-type V_2O_3: A metastable polymorph of vanadium sesquioxide. *Inorg. Chem.* **50**, 6762 (2011).
16. A. Bergerud, R. Buonsanti, J.L. Jordan-Sweet, and D.J. Milliron: Synthesis and phase stability of metastable bixbyite V_2O_3 colloidal nanocrystals. *Chem. Mater.* **25**, 3172 (2013).
17. Y. Xu, L. Zheng, C. Wu, F. Qi, and Y. Xie: New-phased metastable V_2O_3 porous urchinlike micronanostructures: Facile synthesis and application in aqueous lithium ion batteries. *Chem. – Eur. J.* **17**, 384 (2011).
18. A. Bergerud, S.M. Selbach, and D.J. Milliron: Oxygen incorporation and release in metastable bixbyite V_2O_3 nanocrystals. *ACS Nano* **10**, 6147 (2016).
19. C. Reimann, D. Weber, M. Lerch, and T. Bredow: Nonstoichiometry in bixbyite-type vanadium sesquioxide. *J. Phys. Chem. C* **117**, 20164 (2013).
20. C. Wessel, C. Reimann, A. Müller, D. Weber, M. Lerch, T. Ressler, T. Bredow, and R. Dronskowski: Electronic structure and thermodynamics of V_2O_3 polymorphs. *J. Comput. Chem.* **33**, 2102 (2012).
21. T. Lüdtke, D. Weber, A. Schmidt, A. Müller, C. Reimann, N. Becker, T. Bredow, R. Dronskowski, T. Ressler, and M. Lerch: Synthesis and characterization of metastable transition metal oxides and oxide nitrides. *Z. Kristallogr.* **232**(1–3), 3–14 (2017).
22. S. Nakhal, D. Weber, E. Irran, M. Lerch, B. Schwarz, and H. Ehrenberg: Synthese und Kristallstrukturen der neuen Metall-lfluoridhydrate $V_2F_6{\cdot}4H_2O$ und $Mn_3F_8{\cdot}2H_2O$. *Z. Anorg. Allg. Chem.* **636**, 2061 (2010).
23. M. Hölzel, A. Senyshyn, and O. Dolotko: SPODI: High resolution powder diffractometer. *Journal of Large-Scale Research Facilities* **1**, A5 (2015).
24. M. Hölzel, A. Senyshyn, N. Jünke, H. Boysen, W. Schmahl, and H. Fuess: High-resolution neutron powder diffractometer SPODI at research reactor FRM II. *Nucl. Instrum. Methods Phys. Res., Sect. A* **667**, 32 (2012).
25. J. Rodriguez-Carvajal: Recent advances in magnetic structure determination by neutron powder diffraction. *Physica B* **192**, 55 (1993).
26. J. Rodriguez-Carvajal: Recent developments of the program FULLPROF. *Commission on Powder Diffraction Newsletter* **26**, 12 (2001).
27. N.S. Kini, A.M. Strydom, H.S. Jeevan, C. Geibel, and S.J. Ramakrishnan: Transport and thermal properties of weakly ferromagnetic Sr_2IrO_4. *J. Phys.: Condens. Matter* **18**, 8205 (2006).
28. L. Vočadlo, K.S. Knight, G.D. Price, and I.G. Wood: Thermal expansion and crystal structure of FeSi between 4 and 1173 K determined by time-of-flight neutron powder diffraction. *Phys. Chem. Miner.* **29**, 132 (2002).
29. *Semiconductors, 'Non-Tetrahedrally Bonded Binary Compounds II'*, Landolt-Börnstein, Group III Condensed Matter Subvolume D, Vol. **41**, O. Madelung, U. Rössler, and M. Schulz, eds. (Springer, New York, USA, 1969).
30. E.F. Bertaut: Representation analysis of magnetic structures. *Acta Crystallogr., Sect. A: Cryst. Phys., Diffr., Theor. Gen. Crystallogr.* **24**, 217 (1968).
31. E. Hovestreydt, I. Aroyo, S. Sattler, and H. Wondratschek: KAREP—A program for calculating irreducible space-group representations. *J. Appl. Crystallogr.* **25**, 544 (1992).
32. G. Shirane: A note on the magnetic intensities of powder neutron diffraction. *Acta Crystallogr.* **12**, 282 (1959).
33. H. Lueken: *Magnetochemie. Eine Einführung in Theorie und Praxis* (Teubner, Stuttgart, Germany, 1999).